ANNALS OF GEOPHYSICS, 63, 5, PA545, 2020; doi:10.4401/ag-7982

Investigation of the characteristics of geoelectric field earthquake precursors: a case study of the Pingliang observation station, China

Zhanghui An*[,1,2], Yan Zhan[3], Yingying Fan[1,2], Quan Chen[1,2], Jun Liu[1,2]

(1) Gansu Lanzhou Geophysics National Observation and Research Station, Lanzhou 730000, China
(2) Gansu Earthquake Agency, China Earthquake Administration, Lanzhou 730000, China
(3) State Key laboratory of Earthquake Dynamics, Institute of Geology, China Earthquake Administration, Beijing 100029, China

Article history: received October 17, 2018; accepted May 7, 2019

Abstract

An increasing number of earthquake precursors have been observed by geoelectromagnetic stations; however, the statistical characteristics of the earthquake and geoelectric field (GEF) are not well known. Based on the sliding correlation method (SCM) and its validity test, we analyzed 125 months of continuous data from the Pingliang (PL) GEF station in China. Two factors, seismic energy and epicentral distance (D), were used to select the earthquake events. When the lower limit of the magnitude energy is set as 10^6 J/km^2, the number of earthquake events in area A ($D < 200$ km) is 36, and the number of seismic events in area B ($200 \text{ km} \leq D < 365$ km) is 34. In the analysis of the calculated results, the mean value of 1000 times random test SCM calculation is taken as the anomaly standard. In addition, it is found that the anomalies occurring north-south, and north-east of PL station are the most significant in area A, and the anomalies are concentrated approximately 8-26 days before the earthquakes. There is no obvious correlation east-west of PL station in area A, and there is no similar abnormal phenomenon in area B. The reasons and probably mechanism of the investigation results are analyzed and discussed in combination with the fault belt features of the study area, numerical simulation, and laboratory rock fracturing experiments. The uniqueness of the results is verified by reducing the energy standard of a single earthquake. This investigation supports the statistical point of view of the microcosmic interpretation of GEF abnormalities, provides significant suggestions for the selection of electrode-layout orientations used for GEF observations and also provides a reference for the gathering of the seismic precursor information.

Keywords: The geoelectric field (GEF), Statistical characteristic, Shifting correlation method, Correlation coefficient, Earthquake precursor.

1. Introduction

Before and during earthquakes, seismic electromagnetic signals can be produced. These signals have been widely recognized by researchers [e.g. Varotsos et al., 1981; Varotsos and Alexopoulos, 1984a; Park et al., 1993; Huang, 2002, 2005, 2011; Tang et al., 2010; Uyeda et al., 2009]. The geoelectric field (GEF) is mainly used to observe and study anomalous phenomena related to earthquakes. Under normal conditions, for example no man-made disturbance or space electromagnetic activity etc, spectrum analysis results show that the GEF not only reveals the tidal components of different periods, e.g., full day and half days [e.g. Huang and Liu, 2006; Tan et al., 2012], it also reveals the characteristics of seasonal variations [Cui et al., 2013].

After earthquakes have occurred, we can compare their occurrence with the normal conditions to conduct a retrospective investigation of the earthquake events. It is suspected that the anomalous variation phenomenon is related to the earthquake, e.g., the distortion of the waveforms of the GEF before the earthquakes and the fact that the low frequency components of the GEF increase in power (DC-ULF) before earthquakes [Uyeda et al., 2002; Eftaxias et al., 2001; Fan et al., 2010; An et al., 2011, 2013]. Related analysis of the retrospective test of typical earthquake events has been conducted. The number of suspected anomalous GEFs related to earthquakes is limited by the number of earthquake samples and lacks universality or statistical significance. In particular, the statistical correlation between the timing of the GEF anomalies and that of earthquakes is still unclear.

The process of earthquake occurrence caused by the rupture of underground medium is a very complicated geodynamic process, which is accompanied by various physical phenomena, one of which is the electromagnetic anomaly that occurs before the earthquake [Huang, 2005; Thanassoulas, 2007; Orihara, 2012]. At present, because the physical mechanism of the anomalous variation of the GEF before the earthquake is still unclear, statistical analyses may be another feasible method to study the statistical correlation between the GEF and an earthquake event. Earlier statistical studies [Thanassoulas and Tselentis, 1993; Ifantis et al., 1995, 1997; Ifantis, 2002] show that the observation stations a certain distance from the epicenter may detect the low frequency (24±8h) component enhancement before an earthquake. Recent statistical studies [Sarlis, 2018] have also shown that the anomalous GEF phenomena are statistically significant earthquake precursors with lead times in four distinct periods: 3 to 9 days, 18 to 24 days, 43 to 47 days and 58 to 62 days.

In this paper, a sliding correlation method (SCM) [Jiang et al., 2016] based on statistical significance is introduced and used to investigate the correlation between the variation in the diurnal energy of the GEF and the energy of the earthquake events. We use data from the Pingliang (PL) GEF station in the Gansu Province of China. The statistical characteristics of the anomalous occurrence time of GEFs during earthquakes are analyzed. First, the methods of GEF observation, the performance of the observational instruments, and the principles of seismic event selection are introduced. Then, the SCM is briefly introduced, and the validity of the method is verified using a random signal. Last, the results of the investigation are analyzed and discussed in conjunction with the structural characteristics of the fault zone in the investigation area, a numerical simulation of the GEF anomalies, and laboratory rock fracturing experiments.

2. GEF Observation and Earthquake Selection

2.1 Introduction of GEF observation

According to the Greek VAN method [Varotsos et al., 1981], it is possible to capture the precursor information for earthquakes by measuring the GEF. The PL station (35°54'N, 106 °56'E, elevation 1357 m) is located in the Gansu province of China, the small structures around the station are very well developed, mainly in the Liupanshan active fault zone. The strata mainly contain continental rocks and igneous rocks are exposed in some areas.

The observation system used by the PL station adopts an L-shaped pattern (Figure 1a), and the observation channels are aligned in the north-south (NS), east-west (EW), and north-east (NE) directions. Along each of these directions, long and short electrode tracks were installed (Figure 1b) with a long polar distance of 300 m and a short polar distance of 200 m. The measuring electrode is a solid nonpolarized electrode (Figure 1c), and its related parameters are presented in Table 1.

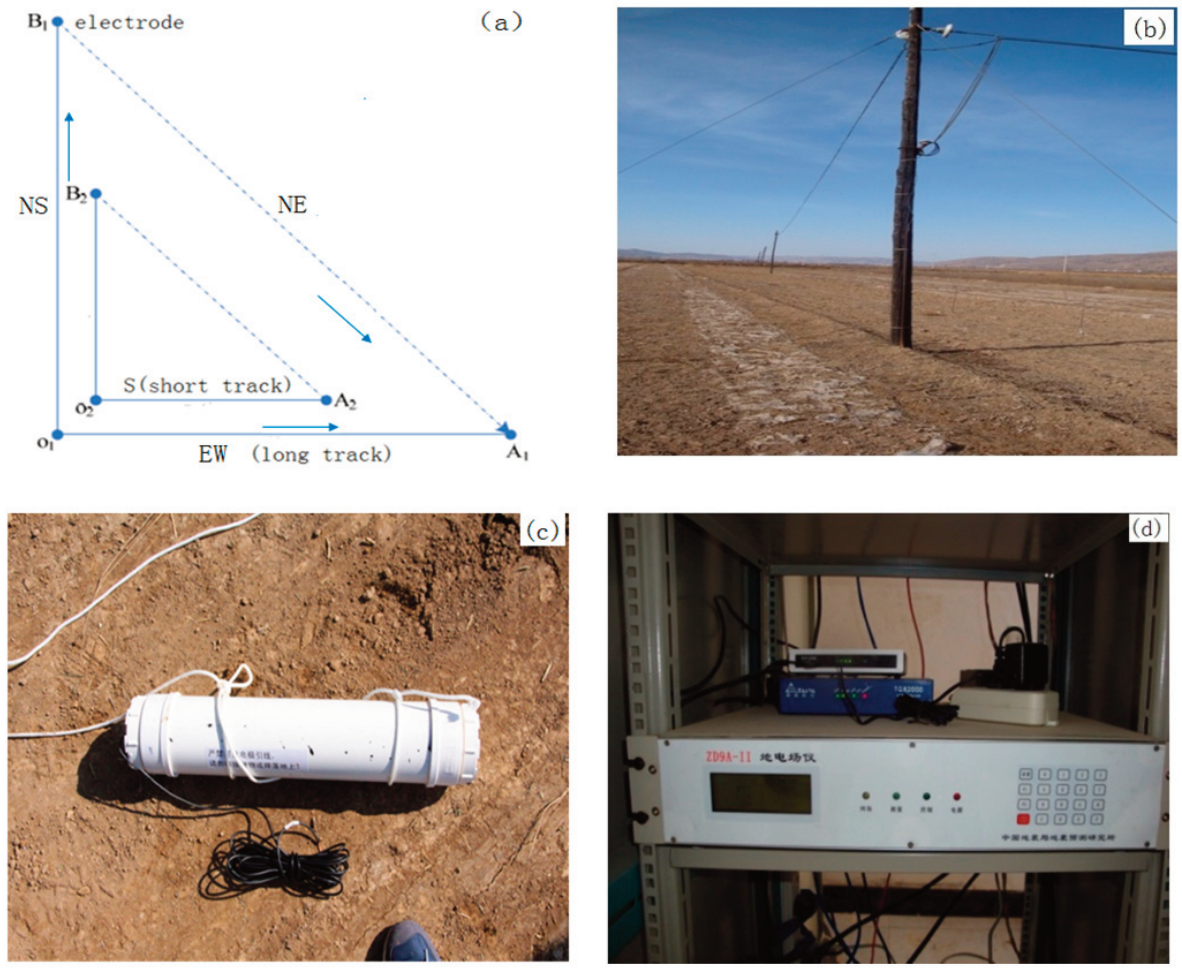

Figure 1. The electrode layout pattern (a), O_1/O_2 electrode position and partial external circuit (b), electrode (c), and observational instruments (d) used by the PL station.

Polarization potential difference of a pair of electrodes	Frequency response range	Electrode internal resistance	Short-term error over 10 seconds	Internal range drift (24 h)	Temperature range
< ±1 mV	0-10 kHz	< 500 Ω	< ±0.01 mV	< ±0.5 mV	–10°C –40°C

Table 1. The main parameters of the solid impolarization electrode (LGB-3), (5% NaCl solution at room temperature).

The burial depth of the electrodes is approximately 3.5 m. The data acquisition instrument is a special digital observation instrument (zd9a- II digital GEF instrument, as shown in Figure 1d) developed and produced by the Institute of Earthquake Forecasting, China Earthquake Administration. The relevant parameters for this instrument are presented in Table 2.

Measurement accuracy	Measurement resolution	Band range	Measurement range	Dynamic range	Sampling rate
< ±(0.1% reading+ 0.02% full scale)	< 10 μV	DC ~0.005 Hz	±1000.000 mV	≥ 100 dB	1 min

Table 2. The main parameters of the digital GEF instrument (ZD9A-II)

The observation was interrupted taking into account device maintenance, instrument faults, power failures, etc. Under normal conditions, the observation station operates non-stop year round. When the observation curves exhibited step or irregular variations, the relevant personnel conducted an inspection and recorded the results in accordance with regulations. The monthly correlation coefficients of the long and short polar distances of PL station are all greater than 0.85. The observation area of the station has a good environment, which provides high quality observation data for our investigation.

2.2 GEF data processing (E series)

The data collection started in January 2008 and ended in May 2018 (3804 days). In cases where the original observation data were deleted due to lightning, human activities, etc., based on the pre-processed observation data, the daily mean energy E_{en} of the GEF was calculated. All of the daily mean energies constitute the GEF time series (E series) used in the analysis with the length of 3804 days. The corresponding formulas are as follows:

$$E_{en} = \log 10\left(\frac{1}{N}\sum_{1day} E_i\right)^2 \qquad \begin{cases} i = 1, 2, 3, ..., N \\ N \le 1440 \end{cases} \tag{1}$$

where E_i is the measured GEF value at the ith minute, in mV/km. N is the number of data per day (local time), at the normal condition N equal to 1440. After the preprocessing and calculations were conducted, the daily energy curves of the three channels at PL station were plotted (Figure 2). The abscissa represent time, the ordinate represent energy, and different colored curves represent different channels, i.e., pink represents NS, blue represents EW, and green represents NE.

Based on the remote reference station theory of magnetotelluric sounding, the correlation between two stations in the same direction was analyzed using the Shandan (SHD) GEF station (the reference station) in Gansu Province, which is approximately 610 km from the PL GEF station (Figure 3). The results show that the correlation coefficients of the NS and EW directions of two stations are 0.851 and 0.777, respectively. The strong correlation show the observational data of PL GEF station have high accuracy in normal condition, the main proportion of data may be dominated by the same external source, while the local electric field induced by the streaming-electrokinetic phenomena [Corwin and Morrison, 1977; Fitterman, 1978], piezostimulated phenomena [Varotsos, 2005; Varotsos and Alexopoulos, 1984a,1986], or rock fracturing phenomena [Ogawa et al., 1985], etc., has a small proportion.

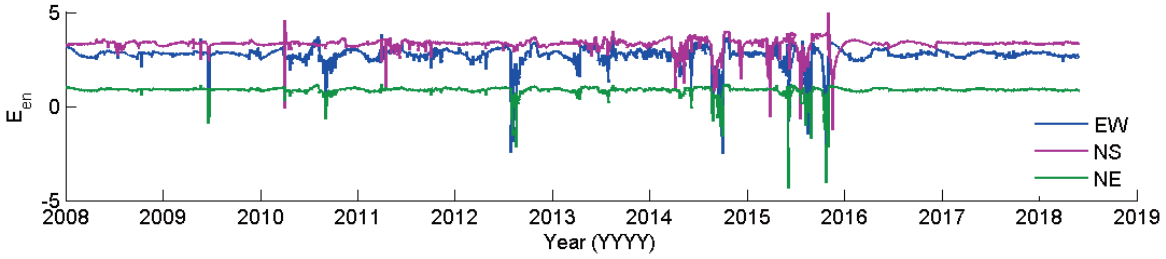

Figure 2. The daily mean energy curves for the PL station.

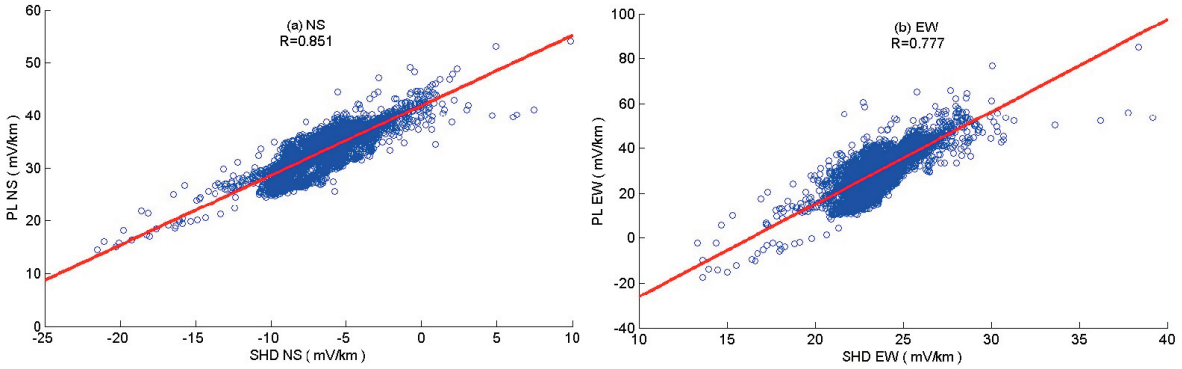

Figure 3. The correlation between PL and SHD stations for the NS and EW channels. The red line is the fitting line; the blue dots represent the correlation coefficient.

2.3 Seismic event processing (M series)

Whether a GEF station can observe earthquake anomalies is dependent on the magnitude of the earthquake's energy and the epicentral distance (D) [Zhuang et al., 2005; Zhao et al., 2009]. In the process of selecting earthquake events, two factors, seismic energy and D, are considered, and the calculation method of determining seismic energy presented by Gutenberg and Richter [1956], Hattori et al. [2006], and Han et al. [2014] is adopted. Equation (2) is used to calculate the energy of a single earthquake event, and Equation (3) is used to calculate the sum of the seismic energy of each day.

$$M_{en,i} = \frac{10^{4.8+1.5}}{Mi} \qquad i = 1, 2, 3, ..., N. \tag{2}$$

$$M_{en,i} = \sum_{1day} M_{en,i} \qquad i = 1, 2, 3, ..., N_{day}. \tag{3}$$

where $M_{en,i}$ is the energy released by the i-th earthquake in J/km^2; M_i is the magnitude of the ith earthquake; D_i is the epicentral distance of the ith earthquake in km, N is the total number of earthquake events, and M_{en} and N_{day} represent the total energy released and the number of earthquakes in one day, respectively. In order to improve the reliability of the results, the energy limit of a single earthquake event should be 10^6 J/km^2. That is to say, the minimum magnitude considered for an epicentral distance of 100 km is 3.5.

We will fill it with '0' when do not have earthquake event in someday, after the logarithm of the daily energy (M_{en}) calculation results in all time periods is taken, the earthquake event sequence (M series) used in the study is constructed. Because we want to study the characteristics of GEF before and after earthquakes for two months (total 121days), so, the maximum length of calculated series is 3683 days.

In this paper, the distributions of seismic events in two regions (A and B) take into account the fact that the seismic energy should exceed the energy limit of 10^6 J/km^2, and the number of seismic events in the two areas should be similar in order to facilitate the comparison about the results. In accordance with these requirements, the final number of qualified earthquakes in area A is 36 and the number in area B is 34. The selected information for seismic events is shown in Tables 3 and 4. The original earthquake catalogue was obtained from the China Earthquake Datacenter (http://data.earthquake.cn). The locations of GEF stations, earthquakes, and faults are shown in Figure 4.

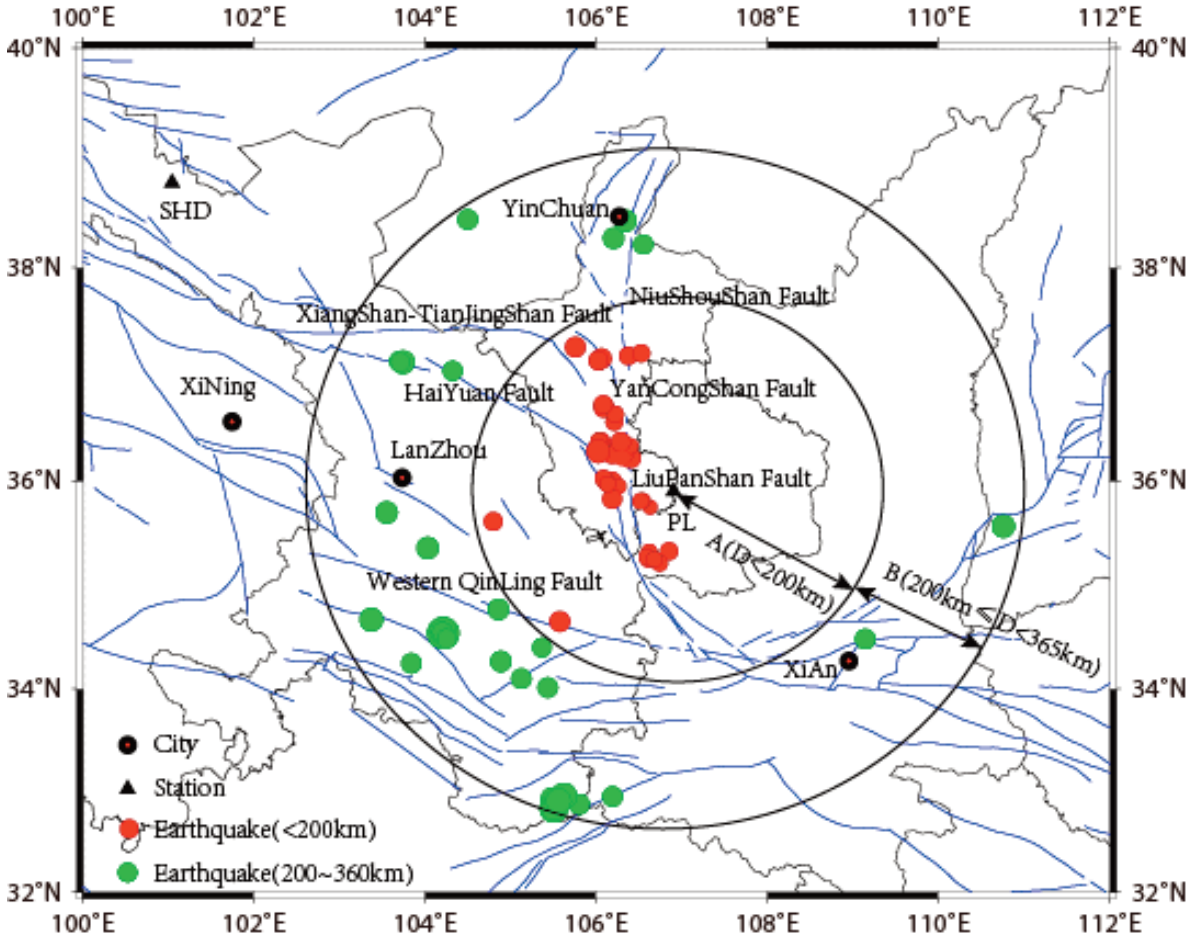

Figure 4. Map showing the GEF station, epicenters, and faults in the target area. The red dots represent seismic activity in area A ($D < 200$ km); the green dots represent seismic events in area B ($200 \text{ km} \leq D < 365$ km); the triangle represents the GEF station; the black circles represent cities; and the blue curves represent faults.

No.	DD-MM-YY	Lat. (°N)	Long. (°E)	Depth (km)	Dist. (km)	Mag. (M)	M_{en}' (lg)
1	14-Feb-08	35.33	106.85	27	63.54	3.7	6.74
2	11-Mar-08	37.18	106.37	25	150.00	3.8	6.15
3	06-Apr-08	36.22	106.40	30	57.32	4.3	7.73
4	06-Apr-08	36.25	106.33	15	64.33	3.5	5.50
5	24-May-08	36.33	106.40	10	65.60	3.3	6.12
6	12-Jun-08	35.75	106.63	12	29.51	3	6.36
7	02-Oct-08	35.99	106.18	6	65.58	4.2	7.47
8	03-Oct-08	35.99	106.12	24	70.93	3.6	6.50
9	24-Nov-08	36.25	106.19	14	74.74	4.5	7.80
10	09-Feb-09	35.29	106.62	8	72.40	3.7	6.63
11	01-Apr-09	36.56	106.21	7	96.00	3.6	6.23
12	05-Apr-09	35.21	106.74	8	78.08	3.4	6.11
13	25-May-09	37.20	106.52	10	148.48	3.7	6.01
14	03-Aug-09	35.25	106.61	7	76.89	3.4	6.13
15	19-Nov-09	35.32	106.62	7	69.28	3.3	6.07
16	20-Nov-09	37.15	106.06	8	157.96	4.2	6.70
17	14-Jan-10	35.28	106.59	7	74.42	3.4	6.16
18	06-Feb-10	35.25	106.68	6	74.97	3.4	6.15
19	26-Apr-14	37.13	106.02	6	157.77	4	6.40
20	04-Feb-15	36.70	106.09	8	114.81	4.2	6.98
21	23-Mar-15	35.95	106.26	9	57.90	3.2	6.07
22	09-Apr-15	34.65	105.57	17	184.10	4.3	6.72
23	28-May-15	35.81	106.54	15	33.95	3.1	6.39
24	01-Jun-15	36.02	106.08	5	75.00	3.6	6.45
25	19-Jul-15	35.62	104.80	12	192.02	3.9	6.08
26	12-Jan-16	36.37	106.28	6	76.36	4.1	7.18
27	11-Apr-16	37.26	105.76	6	182.29	4.3	6.73
28	23-Apr-16	35.83	106.19	6	64.45	4.1	7.33
29	27-Apr-16	35.81	106.52	6	35.68	3.4	6.79
30	24-Apr-17	36.37	106.05	6	92.51	4	6.87
31	14-May-17	36.37	106.03	5	94.00	3.6	6.25
32	01-Sep-17	36.28	106.02	8	89.65	4.9	8.24
33	25-Sep-17	36.63	106.22	8	101.52	3.6	6.19
34	06-Nov-17	35.97	106.13	6	69.76	3.4	6.21
35	12-Nov-17	36.22	106.30	10	64.61	3.3	6.13
36	02-Feb-18	36.72	106.08	7	117.10	3.9	6.51

Table 3. List of major earthquakes in area A.

No.	DD-MM-YY	Lat. (°N)	Long. (°E)	Depth (km)	Dist. (km)	Mag. (M)	M_{en}' (lg)
1	04-Mar-08	35.70	103.55	23	302.93	4.6	6.74
2	12-May-08	32.93	105.48	0	355.00	4.5	6.45
3	27-May-08	32.87	105.50	0	360.57	7.7	8.29
4	10-Jun-08	32.87	105.80	8	351.71	4.8	6.85
5	23-Jul-08	32.83	105.50	4	364.74	5.9	8.53
6	24-Jul-08	32.83	105.50	0	364.74	5.3	7.61
7	11-Sep-08	32.95	105.62	6	348.39	5.8	8.45
8	19-Sep-09	32.90	105.56	8	355.51	5.6	8.04
9	27-Oct-09	37.13	103.70	4	316.97	4.3	6.25
10	04-Nov-09	34.48	109.14	5	257.60	4.7	6.99
11	21-Nov-09	38.21	106.55	6	258.73	4.6	6.85
12	24-Jan-10	35.57	110.76	8	350.31	5.2	7.52
13	22-Jun-10	38.27	106.20	6	270.75	4.9	7.21
14	09-Oct-10	32.95	106.19	8	334.42	4.2	6.05
15	23-Feb-11	34.25	103.84	8	333.45	4.7	6.76
16	01-Nov-11	34.54	104.22	7	286.58	4.9	7.29
17	20-Nov-12	38.43	106.34	21	285.66	5	7.43
18	24-Jan-13	38.44	104.50	6	353.51	4.2	6.00
19	21-Jul-13	34.54	104.21	15	287.35	6.9	10.21
20	22-Jul-13	34.55	104.23	6	285.21	4.3	6.34
21	22-Jul-13	34.56	104.21	14	286.16	5.9	8.75
22	22-Jul-13	34.55	104.20	6	287.53	4.2	6.18
23	28-Jul-13	34.55	104.20	10	287.53	4.6	6.76
24	20-Oct-13	34.49	104.25	7	287.32	4.5	6.63
25	14-Nov-14	37.12	103.74	9	313.29	5.3	7.75
26	02-Dec-14	34.01	105.43	17	249.22	4.2	6.31
27	21-Dec-14	34.40	105.36	10	217.76	4	6.12
28	15-Apr-15	35.36	104.03	9	266.23	5	7.49
29	15-Jul-15	37.12	103.71	14	315.71	4.5	6.54
30	18-Dec-15	34.10	105.12	20	257.57	4.2	6.28
31	17-Jan-16	34.27	104.88	13	258.12	4.4	6.58
32	07-May-16	34.77	104.86	14	223.67	4.4	6.70
33	29-Jul-16	37.04	104.32	13	263.22	4.1	6.11
34	31-Oct-17	34.67	103.37	10	348.35	4.9	7.07

Table 4. List of major earthquakes in area B.

3. Data Analysis Method

The occurrence of an earthquake event is a very complicated geodynamic process, and the anomaly phenomenon before the earthquake varies. However, earthquakes are caused by tectonic movement with similar geodynamic process. For all earthquakes, or all earthquakes of a specific type, the corresponding anomalies related to earthquakes may share similar temporal distribution characteristics[Fan and Che, 2002; Zhang et al., 2005]. Correlation analysis is a basic statistical tool. GEF anomalies may occur before or after an earthquake, i.e., there may be synchronous or asynchronous correlation between earthquake events and GEF observations. In this paper, the SCM is used to investigate the statistical characteristics of seismic anomalies in the GEF.

3.1 Method introduction

In this paper, the earthquake energy sequence (M series) relative to the GEF energy series (E series) sliding by day and calculate the correlation coefficient (R series) between them. In the process of calculation, E_i derived from the E series and it's length is same with M series, we make E_i series fasten and then make M series slide to the left or right, and calculate the correlation coefficient (R_i) each step. When the earthquake and the GEF anomaly occur simultaneously, the R of the two series (M and E_i) can be calculated without relative sliding. When the GEF anomaly occurs before the earthquake, it is necessary to slide the M series to the left, and the calculated R represents the correlation before the earthquake, otherwise, it is necessary to slide the M series to the right, and the R represents the correlation after the earthquake. The correlation coefficient of the two series is as follows:

$$R_{ME_i}=\frac{\sum_{k=}^{m}(M_k-\overline{M})(E_{i,k}-\overline{E}_i)}{\sqrt{\sum_{k=}^{m}(M_k-\overline{M})^2}\sqrt{\sum_{k=}^{m}(E_{i,k}-\overline{E}_i)^2}} \qquad i\in[-60,60]. \tag{4}$$

where M and E_i are the same length (E_i is derived from the long sequence, and M is the short sequence), i is the serial number. $E_{i,k}$ and M_k are the kth sampling values in the E_i and M series, respectively, and $\overline{M}$ and $\overline{E}$are the corresponding average values. In this paper, m is the length of the two equal time series in the calculation, m =3683. R_{ME_i} is the ith correlation coefficient. Through the relative sliding of the two series, we can obtain the continuous change of the correlation coefficient.

3.2 Validity verification

A long sequence containing 301 samples is randomly generated, with a minimum value of 1 and a maximum value of 8, as shown in Figure 5a. Two subsequences, E1[50:90] and E2[180:220], were selected, and the M time series (Figure 5b) was obtained through the average calculation, so the information in subseries E1 and E2 is included in M. According to the theory and calculation of the SCM, the M time series slid to the left or right of E. When M slides to the location of E1 or E2, the calculated correlation is more significant than for other positions. Figure 5c shows the results of the 90 data points of the left and right slipping data and demonstrates that the correlation coefficient increases relative to the position of E1 and E2. Therefore, this method can accurately determine the position of correlated signals in different time series, which verifies the validity of the SCM.

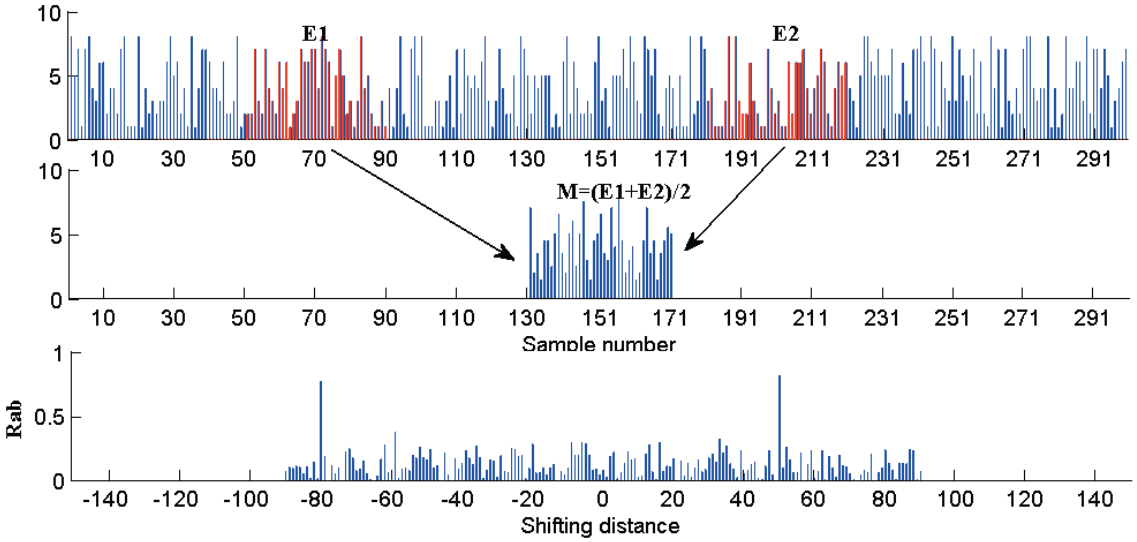

Figure 5. Results of recognition of the random sequence using the SCM.

4. Random test and Discussion

All stages of an earthquake, preseismic, coseismic and postseismic, may be accompanied by an abnormal GEF. The R series reflects the dynamic correlation characteristics of the two time series (M and E_i) and shows the time difference between them. By using the time difference of R series, the statistical characteristics of the GEF observation and the earthquake occurrence time response can be obtained. This can aid in the application of the statistical characteristics to actual investigation and work.

4.1 Random test

The SCM was used to analyze the daily mean energy of the PL GEF from January 2008 to May 2018. The method of earthquake selection is described in section 2.3. Figures 6 and 7 show the results for areas A and B, respectively. The abscissa indicates the relative number of sliding days. The "0" value represents the day of the earthquake. The correlation coefficient at that time reflects the synchronous correlation between the GEF and the earthquake. The negative values of the abscissa indicate the correlation (left slip) before the earthquake, while the positive value indicates the correlation (right slip) after the earthquake. The ordinate is the sliding correlation coefficient of the two time series. The different color curves represent the sliding correlation results of the GEF in different directions, and the corresponding color lines represent the average value of 1000 times random test.

In this paper, the random test is performed, that is, the random disorderly operation of the catalogue and the SCM calculation are carried out, and the mean value of the correlation coefficient obtained by repeating this process 1000 times is taken as the criterion for the deterministic anomaly. When three or more consecutive points exceed this criterion, they are regarded as significant abnormal points. As can be seen from Figure 6, the seismic events located in area A have a good correlation with the GEF. The anomalous correlation coefficient phenomena are concentrated along the NS and NE directions; the anomalies occurred approximately 8-26 days before the earthquake and approximately 20 days after the earthquake. However, the anomalies are not continuous before or after the earthquake in the EW direction. Compared with area A, the characteristics of the correlation anomalies of the three channels in area B are not significant. However, approximately 16-26 days before the earthquake and 40-55 days after the earthquake, a suspected abnormal phenomenon occurs in the NS and EW directions, but there is no abnormal phenomenon in the NE channel at this time.

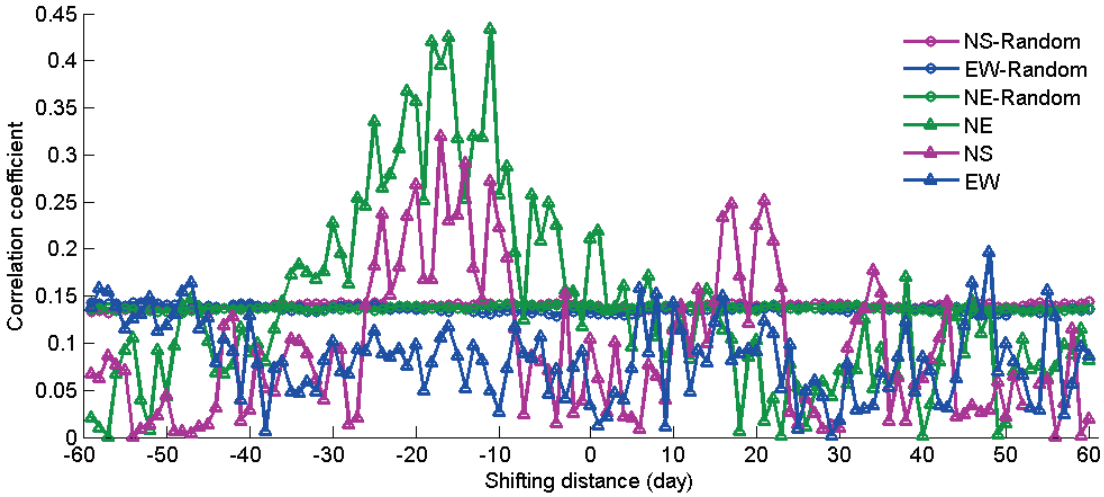

Figure 6. The SCM correlation coefficient curves for the PL station in area A. Pink represents the NS channel; blue represents the EW channel; and green represents the NE channel.

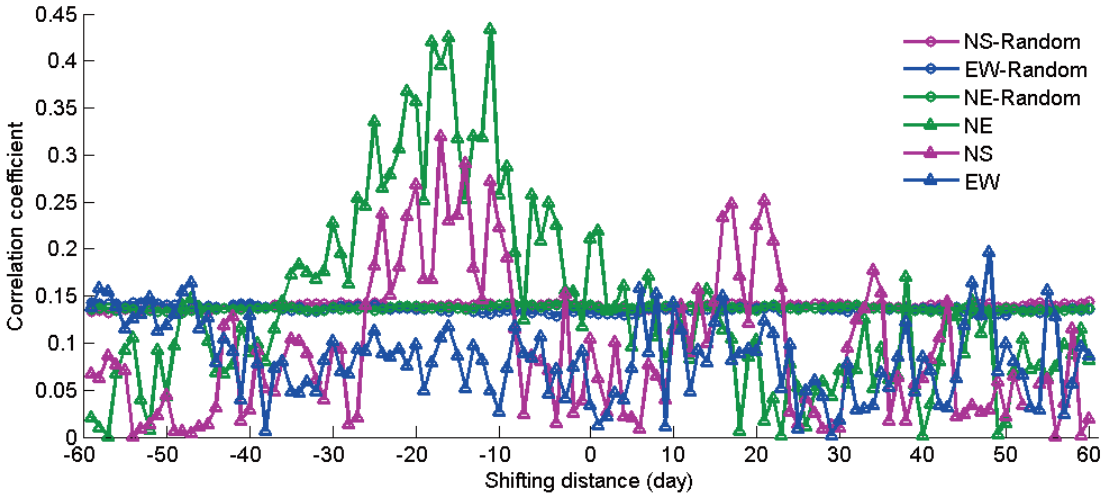

Figure 7. The results of the SCM method for the PL station in area B. Pink represents the NS channel; blue represents the EW channel; and green represents the NE channel.

4.2 Discussion

From the correlate coefficient result of PL and SHD station, we can concluded that the external source is the main proportion of data, so when analyzing the GEF data special attention should be paid to the magnetic influence. Usually, the magnetic influence will be record in all channels of GEF station [Zhang et al., 2006], if the results above are affected by the magnetic storm, then the abnormal characteristics of three channels should have some similarity. In fact, the anomalies only appeared in the NS and NE, and there is no similar phenomenon in the EW channel.

Therefore, it is deduced that our results obtained in this paper do not influence from the same external source (such as magnetic storm).

Compared with area A, there is no similar concentrated anomaly in area B, which may be due to the distance from the observation station to the epicenter of the seismic event, i.e., the seismic event is far away from the epicenter of the observation station, or due to the earthquake events located in different faults. For 16 out of 34 earthquakes, D is greater than 300 km, and the tectonic stress induced by these earthquakes is not enough to cause anomalies in the GEF at a long distance. Alternatively, because the property of the seismogenic fault in area B is different [Zhang et al., 2010; Wu et al., 2016], which leads to a lack of correlation between the GEF and the earthquake.

Although the results for area A show that the GEF has a concentrated anomaly with the seismic events, but the anomaly appears significant directional differences. The correlation features of the NS and NE channels are very similar, while the EW channel finding has almost no correlation features. Combined with the analysis of the geological structure of area A, it is concluded that the geological structure of this area is very well developed [Xie et al., 2000], and the selected seismic events are concentrated on active faults such as the HaiYuan-LiuPanShan fault, the XiangShan-TianJingShan fault, and the YanCongShan fault. The strikes of these fault zones are primarily NS or NE and the maximum principal compression stress direction is NEE-SWW [Dai and Xu, 2016]. The existence of these faults makes the surface inhomogeneity of resistivity, or forms a particular channel for conducting electricity, which leads to the direction selectivity characteristics of the anomalous GEF before the earthquake [Huang and Lin, 2010].

In terms of the microcosmic mechanism, one explanation is that when the medium of the seismogenic body is close to rupturing, the formation and expansion of the microcracks in the medium and the migration of charged ions in the fluid cause the change in the local electric field along the direction of the rupture of the medium [Varotsos and Alexopoulos, 1984a; Corwin and Morrison, 1977]. Another explanation is that the changes in the tectonic stress affect the formation and migration of the lattice defects in the rocks [Varotsos, 1977] and the fluidity of these free and bound lattice defects [Varotsos and Alexopoulos, 1978]. When the tectonic stress reaches the critical value, the relaxation time of these electric dipoles becomes very small which leads to the directional arrangement of the electric dipoles and the emission of transient electrical signals [Varotsos, 2005; Ma et al., 2009]. Recent studies by means of the analysis in a new time domain termed natural time [Sarlis et al., 2013] reveal that a series of transient electric signals start when the fluctuations of the order parameter of seismicity become minimum [Varotsos et al., 2013].

Laboratory rock fracturing experiments show that electromagnetic radiation is produced during the fracture process, and the frequency ranges from very high frequencies to ultra-low frequencies. The long period radiation signals appear before short period signals [Qian et al., 1998], and these long periodic signals may lead to pre-, co-, and after-seismic correlation coefficient anomalies. In actual observations, many strong earthquakes have recorded electromagnetic radiation signals [Karakelian et al., 2002] during the microcracks and expansion of rocks in the late stage of earthquakes. Moreover, the problem puzzling the researchers, why is 8-26 days before earthquakes and 20 days after earthquakes of GEF anomalous variations occurred. Until now, these questions have not yet been answered clearly or fully. All of these require us to carry out more in-depth research and analysis in the future.

Finally, in order to exclude the magnetic influence and verify the uniqueness of the results for area A, the method of increasing or reducing the single seismic energy standard ($10^{5.5}$ J/km^2) was used to compare the results of the calculation. When the energy standard was raised to $10^{6.5}$ J/km^2, the number of qualified seismic events was only 15, which was not considered. When the energy standard was reduced to $10^{5.5}$ J/km^2, the number of seismic events increased to 59. The sliding correlation results are shown in Figure 8. In the two cases, the results of each test are very similar, and the higher the energy standard of a single earthquake, the more significant the correlation of the calculated results, which is consistent with the fact that earthquakes with larger magnitudes are more likely to cause anomalies. The comparative analysis enhances the reliability and uniqueness of the correlation features of area A.

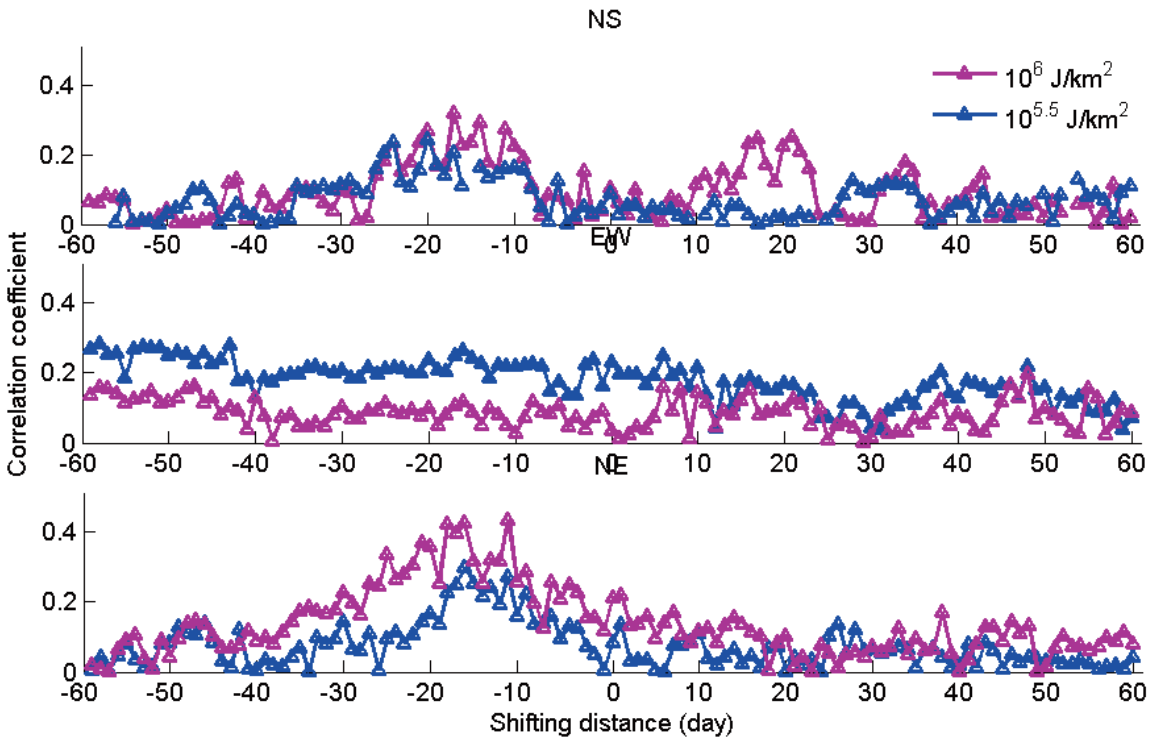

Figure 8. A comparative chart of area A. Pink corresponds to 10^6 J/km^2, and blue corresponds to $10^{5.5}$ J/km^2.

5. Conclusions

By using the improved SCM and 125 months of data from the PL GEF station of China, the statistical characteristics of the GEF and earthquakes in two areas, A and B, were investigated and analyzed. In the earthquake processing part, we take into account the influence of D and earthquake's energy ($\geq 10^6$ J/km^2) 36 earthquakes in area A and 34 in area B are considered. For obtaining reliability anomaly, the average results of 1000 times random test were chosen as the anomaly criterion, the following results were obtained:

For the area A, the abnormal phenomena are appeared along the NS and NE directions, that's centralized appearance approximately 8-26 days before the earthquakes and about 20 days after the earthquakes. But, that's interesting, the similar phenomena are not appeared in the EW direction at the same station. Compared with area A, the anomaly features are not concentrate and synchronous at three channels in area B, that's appeared seemingly 16-26 days before the earthquakes and 40-55 days after the earthquakes, these abnormal phenomenon occurs in the NS and EW directions, but there is no abnormal phenomena in the NE channel this time. The fault features and the earthquakes location in the two areas may be the most reasons, and the reasons worth to investigate deeply.

In addition, it is necessary to note that the limitations of the investigation results obtained in this paper. The statistical characteristics of stations located in different tectonic regions will be different, and the statistical characteristics of each GEF station and the earthquake events will be determined gradually, which can help to improve seismic information capture.

Acknowledgements. We would like to thank the China Earthquake Networks Center for providing observation data for the GEF and earthquake catalogue. We also thank Prof. Chen xiaobin and Dr. Jiang feng (Institute of geology of CEA) for providing the original program, the reviewers for their helpful suggestions, and the editors for their hard work. This work has been supported by the Science for Earthquake Resilience, CEA (grant no. XH16037) and the Basic Scientific Research Special Fund of the Institute of Earthquake Prediction, CEA (grant no. 2012IESLZ04). We would like to thank LetPub (www.letpub.com) for providing linguistic assistance during the preparation of this manuscript.

References

An Z.H., X.B. Du, Y.Y. Fan, J. Liu, D.C. Tan, J.Y. Chen, T. Xie (2011). A study of the electric field before the WenChuan 8.0 Earthquake of 2008 using both space-based and ground-based observational data with spectral element method simulation (in Chinese), Chinese J. Geophys., 54, 6, 818–827, https://doi.org/10.1002/cjg2.1665.

An Z.H., X.B. Du, D.C. Tan, Y.Y. Fan, J. Liu, T.F. Cui (2013). Study on the Geo-electric field variation of Sichuan Lushan Ms7.0 and Wenchcuan Ms8.0 Earthquake (in Chinese), Chinese J. Geophys., 56, 6, 721–730, https://doi.org/10.1002/cjg2.20065.

Corwin R. F., H. F. Morrison (1977). Self-potential variations preceding earthquakes in central California, Geophys. Res. Lett., 4, 4, 171–174, https://doi.org/10.1029/GL004i004p00171.

Cui T.F., X.B. Du, Q. Ye, J. Y. Chen, J.J. Wang, Z.H. An, Y.Y. Fan, J. Liu (2013). The diurnal variation of Geo-electric field along the longitude and latitude chains in China mainland (in Chinese), Chinese J. Geophys., 56, 411–424.

Dai H., J.Xu (2016), Analysis of the GPS Section Deformation and Strain Accumulation of the Eastern Haiyuan and the Western Liupanshan Faults (in Chinese), J. Geod. Geodyn., 36,.4,343-345,349, https://doi.org/10.14075/j.jgg.2016.04.014.

Eftaxias K., P. Kapiris, J. Polygiannakis, N. Bogris, J. Kopanas, G. Antonopoulos, A. Peratzakis, V. Hadjicontis (2001), Signature of pending earthquake from electromagnetic anomalies, Geophs. Res.Lett., 28,.17, 3321–3324, https://doi.org/10.1029/2001GL013124.

Fan Y., Z.H. Che (2002).Characteristics of fault horizontal anomalous movement before earthquakes (in Chinese), Earthquake, 22, 2, 88-93.

Fan Y.Y., X.B. Du, J. Zlotnicki, D.C. Tan, J. Liu, Z.H. An, J.Y. Chen, G.L. Zheng, T. Xie (2010). The electromagnetic phenomena before the Ms8.0 Wenchuan Earthquake (in Chinese), Chinese J. Geophys, 53,.6, 997–1010. https://doi.org/10.1002/cjg2.1570.

Fitterman D (1978). Electrikinetic and magnetic anomalies associated with dilatant regions in a layered earth, J Geophys. Res., 83,B12, 5923–5928. https://doi.org/10.1029/JB083iB12p05923.

Gutengerg B., C.F. Richter (1956). Magnitude and energy of earthquakes, Ann. Geophys., 9, 1–15.

Han P., K. Hattori, M. Hirokawa, J. Zhuang, C.H. Chen, F. Febriani, H. Yamaguchi, C. Yoshino, J.Y.Liu, Yoshida S (2014). Statistical analysis of ULF seismomagnetic phenomena at Kakioka, Japan, during 2001-2010, J. Geophys. Res.: Space Physics, 119, 4998–5011. https://doi.org/10.1002/2014JA019789.

Hattori K., A. Serita, C. Yoshino, M. Hayakawa, N. Isezaki (2006). Singular spectral analysis and principal component analysis for signal discrimination of ULF geomagnetic data associated with 2000 Izu Island Earthquake Swarm, Phys. Chem. Earth, 31, 281–291. https://doi.org/10.1016/j.pce.2006.02.034.

Huang Q., (2002).One possible generation mechanism of co-seismic electric signals, Proceedings of the Japan Academy, Series. B, Physical and Biological Sciences, 78, 173–178. https://doi.org/10.2183/pjab.78.173.

Huang Q., (2005). The state of the art in Seismic electromagnetic observation (in Chinese)., Recent developments in world seismology, 323, 2–5.

Huang Q., (2011). Rethinking earthquake-related DC-ULF electromagnetic phenomena: towards a physics-based approach, Nat. Haz. Earth Sys. Sci., 11, 2942–2949, http://doi.org/10.5194/nhess-11-2941-2011.

Huang Q., T. Liu (2006). Earthquake and tide response of Geoelectric potential field at the Niijima station, Chinese J Geophys., 49(6), 1585–1594, https://doi.org/10.1002/cjg2.986.

Huang Q., Y. Lin (2010). Selectivity of seismic electric signal(SES) of the 2000 Izu earthquake swarm: a 3D FEM numerical simulation model, Proceedings of the Japan Academy, Series. B, Physi. Biol. Sci., 86(3), 257–264, https://doi.org/10.2183/pjab.86.257.

Ifantis A. (2002). A new approach of investigate the correlation between periodicity of geoelectric field and earthquakes, Digit. Signal Process., 905–910.

Ifantis A., A. Tselentis, P.A. Varotsos, C. Thanassoulas (1995). Long-term variations of the earth's electric field preceding two earthquakes in Greece, Int. J. Rock Mech. Min. Sci., 32, 104A.

Ifantis A., G. Economou, S. Despotopoulos, A. Tselentis, T. Deliyannis (1997). Exploratory analysis of electrotelluric field data for earthquake prediction, Digit. Signal Process. 973–976, https://doi.org/10.1109/ICDSP.1997.628526.

Jiang F., X.B. Chen, Y. Zhan, G.Z. Zhao, H.Yang, L.Q. Zhao, L. Qiao, L. Wang (2016). Shifting Correlation Between Earthquakes and Electromagnetic Signals: A Case Study of the 2013 Minxian–Zhangxian M L 6.5 (MW 6.1)

Earthquake in Gansu, China, Pure Appl. Geophys., 173, 269–284, https://doi.org/ 10.1007/s00024-015-1055-4.

Karakelian D., G. C.Beroza, S. L.Klemperer, A.C.Fraser-Smith (2002). Analysis of Ultralow-Frequency Electromagnetic Field Measurements Associated with the 1999 M7.1 Hector Mine, California, Earthquake sequence, Bull. Seismological Soc. Am. 92,.4,1513–1534.

Ma Q., W.G. Zhao, W. Zhang (2009). Abnormal variations of geoelectric field recorded at Wenxian station preceding earthquakes and their application to the prediction of the 2001 MS 8 .1 Kunlun earthquake (in Chinese), Acta Seismologica Sinica, 31, 6, 660–670.

Ogawa T., K. Oike, T. Miura (1985). Electromagnetic radiations from rocks, J. Geophys. Res., 90, D4, 6245–6249, https://doi.org/10.1029/JD090iD04p06245.

Orihara Y., M. Kamogawa, T. Nagao, S.Uyeda (2012). Preseismic anomalous telluric current signals observed in Kozu-shima Island, Japan, Proceedings of the National Academy of Sciences,109(47), 19125-19128. https://doi.org/ 10.1073/pnas.1215669109.

Park S. K., M. J. S. Johnston, T.R. Madden, F.D. Morgan, H. F. Morrison (1993). Electromagnetic precursors to earthquakes in the ULF band: A review of observations and mechanisms, Rev. Geophys., 31, 117–132, https://doi.org/10.1029/93RG00820.

Qian S., K. Ren, Z. Lv (1998). Experimental study of the feature of VLF, MF, HF and VHF electromagnetic radiation accompanying rock fracture (in Chinese), Acta Seismological Sinica, 18, 346–351.

Sarlis N. V. (2018). Statistical significance of earth's electric and magnetic field variations preceding earthquakes in Greece and Japan revisited, entropy, 20, 561, 1-17, https://doi.org/10.3390/e20080561.

Sarlis N. V., E. S. Skordas, P. A.Varotsos, T. Nagao, M. Kamogawa, H. Tanaka, S. Uyeda (2013). Minium of the order parameter fluctuations of seismicity before major earthquakes in Japan, Proceedings of the National Academy of Sciences, 110, 34, 13734-13738, http://doi.org/10.1073/pnas.1312740110.

Tan D.C., J.L. Zhao, J.L. Xi, D.P. Liu, Z.H. An (2012).The variation of waveform and analysis of composition for the geoelectrical field before moderate or strong earthquakes in Qinghai-Tibetan plateau regions, Chinese J. Geophys. 55, 2, 136–149, https://doi.org/10.1002/cjg2.1709.

Tang J., Y. Zhan, L.F. Wang, Z. Dong, G.Z. Zhao, J. Xu (2010), Electromagnetic coseismic effect associated with aftershock of Wenchuan MS8.0 earthquake, Chinese J. Geophys., 53, 526–534.

Thanassoulas C. (2007). Short-term Earthquake Prediction. Greece: H. Dounias & Co.

Thanassoulas C., G.Tselentis (1993). Periodic variations in the earth's electric field as earthquake precursors: results from recent experiments in Greece, Tectonophysics, 224, 103–111, https://doi.org/10.1016/0040-1951(93)90061-N.

Uyeda S., M. Hayakawa, T. Nagao, O. Molchanov, K. Hattori, Y. Orihara, K. Gotoh, Y. Akinaga, H. Tanaka (2002). Electric and magnetic phenomena observed before the volcano-seismic activity in 2000 in the Izu Island Region, Japan, Proc. Natl .Acad .Sci. USA, 99, 7352–7355, https://doi.org/10.1073/pnas.072208499.

Uyeda S., T. Nagao, M. Kamogawa (2009). Short-term earthquake prediction: Current status of seismo-electromagnetics, Tectonophysics, 470, 205–213.,https://doi.org/10.1016/j.tecto.2008.07.019.

Varotsos P. A. (1977). On the temperatue and pressure dependence of the defect formation volume in ionic crystals, J. Physiq. Lett., 38, 455–458.

Varotsos P. A. (2005). The Physics of Seismic Electric Signals. Tokyo: Terra Pub:338.

Varotsos P. A., K. Alexopoulos (1978).Calculation of the migration volume of vacancies in ionic solids from macroscopic parameters, Physica Status Solidi(a), 47, K133–K136.

Varotsos P. A., K. Alexopoulos (1986). Thermodynamics of Point defects and their relation with bulk properties, North Holland, New York, 472.

Varotsos P. A., K. Alexopoulous, K. Nomicos (1981).Seismic electric currents, Praktica Athens Academy, 56, 277–286.

Varotsos P.A., K. Alexopoulos (1984a). Physical properties of the variations of the electric field of the earth preceding earthquakes, I , Tectonophysics, 110,73–98, https://doi.org/10.1016/0040-1951(84)90060-X.

Varotsos P.A., N.V. Sarlis, E.S. Skordas, M.S. Lazaridou (2013). Seismic Electric Signals: An additional fact showing their physical interconnection with seismicity, Tectonophysics, 589,18, 116-125, https://doi.org/10.1016/j.tecto.2012.12.020.

Wu Z., D. Yuan, A. Wang, B. Zhang, Y. Shao, P. Wang (2016), New Evidence for Holocene Tectonic Activities of the Wushan - Tianshui Segment in the Northern Margin Fault of the West Qinling (in Chinese), China Earthq. Engin. J., 28, no.2, 249-259.

Xie F., S. Shu, S. Dou, S. Zhang (2000), Quaternary tectonic stress field in the region of Haiyuan-Liupanshan fault zone to Yinchuan fault-depression (in Chinese), Seismol. Geol., 22, 2, 139-146.

Zhang H., P. Zhang, D. Yuan, W. Zheng, D. Zheng (2010), Differential landscape development of the central N-S seismic zone and its relation to the west Qinling tectonic belt(in Chinese), Quaternary Sci., 30, no.4, 803-811, https://doi.org/10.3969/j.issn.1001-7410.2010.04.15.

Zhang X., J. Guo, X. Guo (2006). Analysis on digital geoelectric field anomalies in Hebie province(in Chinese), Earthquake Res. China, 22,1, 64-75.

Zhang X., Guo X., Guo J. (2005). Geoelectric potential anomalies before earthquakes in the joint areas of Shanxi, Hebei and Inner Mongolia, Seismol. Geol., 27, 3, 420-428. (in Chinese with English abstract).

Zhao G., Y. Zhan, L.Wang, J. Tang, Q. Xiao, X. Chen (2009). Electromagnetic anomaly before earthquakes measured by electromagnetic experiments, Earthquake Sci., 22, 395–402, https://doi.org/10.1007/s11589-009-0395-5.

Zhuang J., D. Vere-Jones, H. Guan, Y. Ogata, L. Ma (2005). Preliminary analysis of observations on the ultra-low frequency electric field in a region around Beijing, Pure Appl. Geophys., 162, 1367–1396, https://doi.org/10.1007/s00024-004-2674-3.

***CORRESPONDING AUTHOR**: **Zhanghui AN**,
Gansu Lanzhou Geophysics National Observation
and Research Station,
Lanzhou 730000, China,
e-mail: anzhanghui5@hotmail.com